Complexity in lipid membrane composition induces resilience to $A\beta_{42}$ aggregation

Michele Sanguanini, Kevin N. Baumann, Swapan Preet, Sean Chia, Johnny Habchi, Tuomas P. J. Knowles and Michele Vendruscolo

Centre for Misfolding Diseases, Department of Chemistry, University of Cambridge, Cambridge CB2 1EW, UK

Supporting Information Placeholder

ABSTRACT: The molecular origins of Alzheimer's disease are associated with the aggregation of the amyloid-β peptide (Aβ). This process is controlled by a complex cellular homeostasis system, which involves a variety of components, including proteins, metabolites and lipids. It has been shown in particular that certain components of lipid membranes can speed up Aβ aggregation. This observation prompts the question of whether there are protective cellular mechanisms to counterbalance this effect. Here, to address this issue, we investigate the role of the composition of lipid membranes in modulating the aggregation process of Aβ. By adopting a chemical kinetics approach, we first identify a panel of lipids that affect the aggregation of the 42-residues form of Aβ ($A\beta_{42}$), ranging from enhancement to inhibition. We then show that these effects tend to average out in mixtures of these lipids, as such mixtures buffer extreme aggregation behaviors as the number of components increases. These results indicate that a degree of quality control on protein aggregation can be achieved through a mechanism by which an increase in the molecular complexity of lipid membranes balances opposite effects and creates resilience to aggregation.

Keywords: Protein misfolding diseases; protein aggregation; cellular homeostasis; protein homeostasis; lipid homeostasis; phospholipids

Introduction

Alzheimer's disease (AD) is increasingly prevalent in our ageing world, and the economic burden of managing this condition is putting national healthcare systems under major stress[1]. The accumulation of extracellular plaques formed of the amyloid-β peptide (Aβ), with a prevalent presence of the 42-residue form of Aβ ($A\beta_{42}$), is one of the hallmarks of AD[2]. In particular, the proliferation of small soluble Aβ aggregates, known as oligomers, has been related to the onset of the disease[3–5]; thus, investigating the mechanisms that govern $A\beta_{42}$ aggregation at early stages may lead to novel strategies to delay or prevent the onset of AD.

Because of the toxicity associated with protein aggregation, living systems have evolved complex quality control mechanisms, collectively known as protein homeostasis system, that reduce the presence of protein aggregates[6,7]. These mechanisms enable the regulation of protein synthesis, trafficking, interactions and degradation, and involve a wide range of cellular components, including enzymes[8], molecular chaperones[6], metabolites[9] and lipids[10], which we are only beginning to understand in detail.

Lipid membranes can influence Aβ aggregation via multiple mechanisms, including surface crowding or templating effects[11]; furthermore some lipids, such as gangliosides, trigger the local formation of toxic, membrane-associated aggregates[12]. It has also been recently shown that cholesterol, an abundant component of lipid membranes in the brain, can speed up Aβ aggregation up to 20-fold through a pathway of heterogeneous primary nucleation[13]. More generally, the physical and chemical properties of lipids strongly can affect the kinetics of the membrane-induced protein aggregation[14–18]. Indeed, an extensive study of about a hundred different lipids reported inhibitory effects on the aggregation of human apolipoprotein C-II in about half of the cases and enhancing effects in the other half, with an approximately Gaussian distribution in the strength of these effects[19]. This result suggests, because of the central limit theorem in probability theory[20], that lipid mixtures could average out the effects of individual lipids.

Table 1. Structure and relevance of the lipid systems studied in this work

Phospholipid	*Structure*	*Detected in brain*	*Relative abundance*
DMPG	14:0-14:0 PG	N.A.	N.A.
POPG	16:0-18:1 PG	Yes	+++
DMPS	14:0-14:0 PS	N.A.	N.A.
POPS	16:0-18:1 PS	Yes	++
POPC	16:0-18:1 PC	Yes	+++
POPE	16:0-18:1 PE	Yes	+

PG: phosphatidylglycerol, PS: phosphatidylserine, PC: phosphatidylcholine, PE: phosphatidylethanolamine. Relative abundance within phospholipids having the same headgroup from Choi et al.[10]; +++: more than 30%, ++: 20 to 30%, +: less than 20%.

Results

In order to study the role of the composition of lipid membranes on $A\beta_{42}$ aggregation, we apply a highly reproducible chemical kinetics assay of $A\beta_{42}$ aggregation[13,21–24] in the presence of small unilamellar vesicles (SUVs)[13] composed of combinations of model and biologically-relevant phospholipids (**Table 1**). Approaches based on chemical kinetics make it possible to characterize *in vitro* the fundamental molecular steps that govern $A\beta_{42}$ amyloid formation[21] and to determine the effects that different molecular species - including small molecules[23], molecular chaperones[24,25], antibodies[26] and amyloid plaques coaggregators[27] - have on $A\beta_{42}$ aggregation.

Phospholipid SUVs production and chemical kinetics measures were performed according to previously published methods[13] (see **Supplementary Information**). Briefly, amyloid formation in presence of different molar excesses of SUVs was monitored in a reaction solution containing 2 μM recombinant $A\beta_{42}$ peptide in 20 mM sodium phosphate buffer (pH 8.0) supplemented with 0.2 mM EDTA and 20 μM thioflavin T (ThT).

We first investigated the effects that SUVs composed of individual species of phospholipids have on $A\beta_{42}$ aggregation (**Figs. 1** and **S1**). We found that different lipid species have opposite effects on the kinetic profiles. Vesicles made of POPE, POPC, and DOPC speed up $A\beta_{42}$ aggregation, reaching saturation at 50-fold molar excess (**Fig. S1**). By contrast, vesicles made of DMPG, POPG, DMPS, and POPS can delay $A\beta_{42}$ aggregation up to four-fold (**Figs. 1** and **S1**). The latter SUVs appear to transiently interact with ThT, thus undergoing an initial equilibration and dampening the fluorescence value of the aggregation plateau, which leads to dramatic aggregation reduction at high SUVs molar excess (**Fig. S2**). We determined an optimal vesicle concentration of 100 μM, which maximizes the effect of a given lipid species on $A\beta_{42}$ aggregation, while minimizing ThT-associated artefacts.

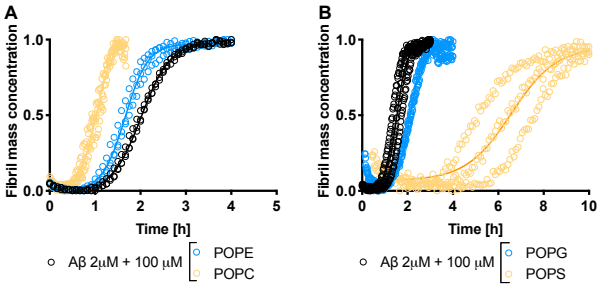

Figure 1. **Comparison of the kinetic effects of different SUVs on $A\beta_{42}$ aggregation *in vitro*.** (A) Some lipid species induce an enhancement of $A\beta_{42}$ aggregation. (B) By contrast, others lipid species induce a delay of this process. The kinetic profiles (solid lines) were derived from triplicates of each sample.

We then asked how combinations of different phospholipid species in the same vesicles influence $A\beta_{42}$ aggregation. Thus, we produced SUVs via mixing equal parts of two phospholipids showing non-neutral effects on $A\beta_{42}$ aggregation. One of three combinations can occur: (i) both lipids accelerate Aβ aggregation, (ii) both delay it, or (iii) they have opposite effects (**Fig. 2**). SUVs composed of phospholipids that induce a delay in Aβ aggregation - either with the same fatty acid composition (POPG:POPS, **Fig. 2A.1** and **S3A.1**), or with the same phosphate head groups (DMPG:POPG, **Fig. 2A.2** and **S3A.2**) - induce a kinetic behavior that is intermediate compared with the effects from the same number of single-lipid vesicles. The same phenomenon can be seen in the case of two phospholipid species that induce an acceleration of $A\beta_{42}$ aggregation (**Figs. 2B** and **S3B**). Likewise, mixing a delaying lipid (POPG) with an accelerating one (POPC) affects the peptide aggregation in a quasi-neutral fashion (**Figs. 2C** and **S3C**). Using differential scanning calorimetry (DSC) and ssDNA-SUV gel electrophoresis, we confirmed the formation of vesicles composed of a mixture of the two lipid species (**Fig. S4**).

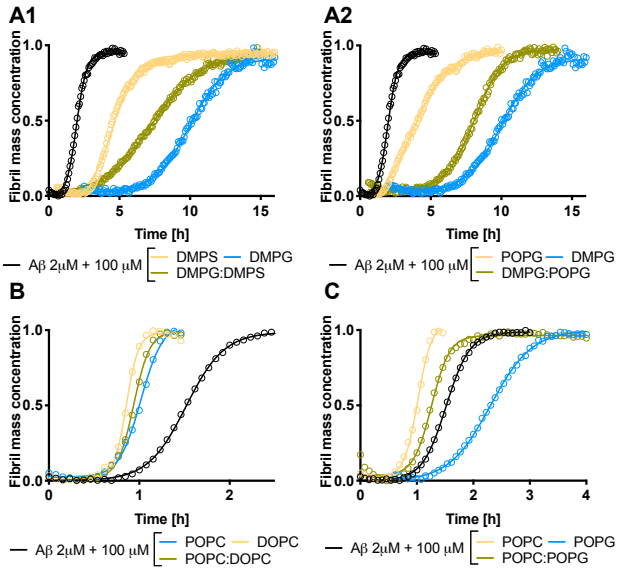

Figure 2. **Binary mixtures of lipids average out the effects on the kinetics of Aβ$_{42}$ aggregation of the individual lipids**. (A) Mixtures of lipids delaying Aβ$_{42}$ aggregation, either showing same fatty acid tails (A1) or phosphate head (A2), induce kinetic profiles which are intermediate when compared to those of pure phospholipid SUVs. (B) The same is true for mixtures of lipids inducing an acceleration of Aβ$_{42}$ aggregation. (C) Mixing lipids with opposite effects on Aβ$_{42}$ aggregation induces an intermediate effect that is closer to the aggregation of Aβ$_{42}$ alone. Average values were derived from a minimum of two technical replicates for each sample.

In order to expand from the previous findings, we performed aggregation kinetics in presence of SUVs derived from more complex lipid mixtures (**Fig. 3**). In order to investigate whether the complexity in the composition of the SUVs can induce systemic resilience to Aβ$_{42}$ aggregation, we first used a 4-lipid model mixture (4LM), composed of equal parts of phospholipids POPE, POPC, POPG, and POPS. As expected from our rationalisation of the results presented above for binary mixtures, we found that this more complex mixture induces a behavior that is an average respective to the behavior of single components (**Fig. 3A**). In this phenomenon, the net result of opposing effects by different lipids is to have membranes that are relatively neutral in terms of their influence on Aβ aggregation.

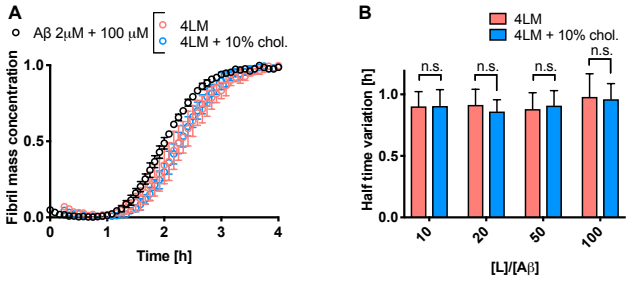

Figure 3. **The complexity in the composition of lipid membranes can induce resilience to Aβ$_{42}$ aggregation**. (A) Representative Aβ$_{42}$ aggregation curves in presence of 4LM SUVs with or without 10% cholesterol. (B) The half-time variation relative to Aβ$_{42}$ (± SEM) shows that the presence of cholesterol and the lipid concentration in solution do not affect the aggregation in a statistically significant way (two-way ANOVA, Bonferroni-corrected for multiple comparisons). Data obtained from three independent experiments.

To understand the mechanisms underlying the averaging effect of lipid mixtures, we asked whether this behavior might be due to the combination of the effects of distinct lipid species (**Fig. S5**). We focused on mixture of anionic systems, such as DMPG:POPG (**Fig. S5A**) and DMPG:DMPS and POPG:POPS (**Fig. S5B-D**), to deter the exchange of phospholipids[28] and formation of hydrogen bonds affecting surface reactivity[29] that might occur with mixing vesicles of opposite charge (**Fig. S4B**). Our results show that the kinetic effects of equal mixtures of lipids show a linear correlation with the effects of adding each lipid in form of pure vesicles up to the same concentration in the mixture (Pearson's correlation coefficient r=0.83, one-tail p=0.0001, **Fig. S4E**).

We note that it is also possible that the averaging effect of lipid mixtures is due to the disruption of higher-level, cooperative structures occurring in the pure phospholipid membranes with stronger effects on Aβ$_{42}$ aggregation. To address this point, we investigated the effect of a physiological concentration of 10% cholesterol, which can induce an increase in Aβ$_{42}$ aggregation via a heterogeneous primary nucleation pathway[13], on 4LM mixtures. Our results show that a complex lipid environment not only exhibits a balancing behavior, but it might also deter the presence of cooperative mechanisms, such as the formation of cholesterol complexes that might underlie Aβ heterogeneous primary nucleation (**Fig. 3B**). This effect, however, does not significantly affect the high-level morphology of Aβ$_{42}$ fibrils, as shown by TEM imaging of the aggregation endpoints (**Fig. 4**). It is, however, known from previous observations that Aβ$_{42}$ fibrils formed in presence of SUVs may incorporate lipids in their structure[13], and liposomes surrounding fibrils are visible in the TEM images (**Fig. 4B,C**).

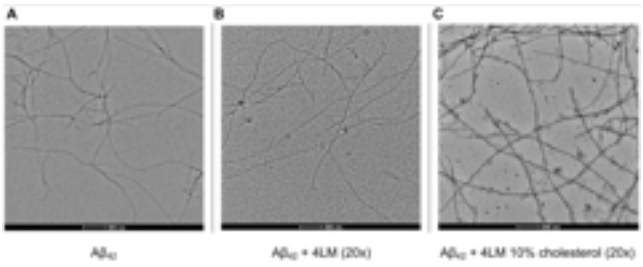

Figure 4. **Similar morphologies of Aβ fibrils in presence of liposomes**. TEM images endpoint fibrils derived from $A\beta_{42}$ (A) in absence of liposomes, (B) in presence of 20-fold excess 4LM liposomes, and (C) in presence of 20-fold excess 4LM liposomes supplemented with 10% cholesterol.

Discussion

In this study, we have illustrated how different phospholipid species can affect the kinetics of $A\beta_{42}$ aggregation in opposite ways, with some families of lipids inhibiting aggregation and other families enhancing it. In particular, under the conditions that we used, PG-containing phospholipids can delay $A\beta_{42}$ aggregation up to five-fold, although under different conditions these lipids can accelerate Aβ aggregation in vitro[11,30]. Although PG is present at low abundance in brain membrane extracts (less than 0.01% in human brain, less than 0.2% in mouse brain)[31,32], a lipidomic study on synaptosomal membrane fractions has shown that PG is selectively enriched at synaptic level in rats[33]. Taken together, these results suggest a scenario where aggregation-delaying lipid species buffer $A\beta_{42}$ aggregation at synapses.

Our central result is that mixing different phospholipids induces an averaging of the effects of the individual components on $A\beta_{42}$ aggregation. Following this finding, we have shown that multi-component membranes exhibit resilience to the emergence of phenomena such as the pathway of heterogeneous primary nucleation triggered by cholesterol[13]. An important consequence of these findings is that increasing complexity of a phospholipid mixture avoids extreme behaviors of $A\beta_{42}$ in presence of lipid membranes and that it provides a degree of protection against aggregation.

In conclusion, we have described an aspect of the lipid homeostasis system that complements the protein homeostasis system to prevent $A\beta_{42}$ aggregation. In this phenomenon, the enhancement effects of $A\beta_{42}$ aggregation of certain lipids is counterbalanced by the inhibitory effects of other lipids. These observations suggest that the complexity of lipid membranes is not only essential for normal cellular functions, but it may also provide an effective protection mechanism against protein aggregation.

Methods

Purification of the $A\beta_{42}$ peptide. The recombinant Aβ (M1-42) peptide (M DAEFRHDSGY EVHHQKLVFF AEDVGSNKGA IIGLMVGGVV IA), here called $A\beta_{42}$, was expressed in the *E. coli* BL21 Gold (DE3) strain (Stratagene, San Diego, CA, USA) and purified as described previously with slight modifications[35]. In a nutshell, the transformed *E. coli* cells were sonicated and the extracted inclusion bodies were dissolved in 8 M urea. The solution was then ion exchanged in batch mode on diethylaminoethyl cellulose resin and lyophilized. These lyophilized fractions were further purified using a Superdex 75 HR 26/60 column (GE Healthcare, Chicago, IL, USA) and the eluates were analyzed using SDS-PAGE to confirm the presence of the desired protein product. The fractions containing the recombinant protein were pooled, aliquoted, frozen using liquid nitrogen, and lyophilized again to obtain the working stock.

Small unilamellar vesicles (SUVs) production. Phospholipid SUVs were produced according to the manufacturer protocol (Avanti Polar Lipids, Alabaster, AL, USA), with minor modifications. Briefly, the chosen quantity of lipids, solubilized in an organic solvent (chloroform or chloroform-methanol according to the manufacturer instructions), was dried using a gaseous N2 line and the lipid film further desiccated under vacuum condition overnight at room temperature. The film was then resuspended at room temperature in 20 mM sodium phosphate 0.2 mM EDTA buffer pH 8.0, frozen in dry ice and thawed at 37 ◦C. Three further freeze-thawing cycles were performed in order to insulate the lipid complexes that are most thermodynamically stable at the working temperature. After the last thawing, the produced multilamellar vesicles were down-scaled to SUVs through sonication (15 minutes in melting ice, 0.5 duty cycle, 25% power) using a Sonopuls HD 2070 sonicator (Bandelin, Berlin, Germany). In order to eliminate bigger particulate derived from the sonication process, the obtained SUVs were centrifuged in a benchtop centrifuge (15 min, 19000×g, room temperature) and the supernatant transferred in a new test tube.

Kinetic assay and thioflavin T (ThT) aggregation time course. In order to prepare a solution of pure monomeric peptide, the lyophilized $A\beta_{42}$ peptide was resuspended in 6 M guanidinium hydrochloride (GuCl) and then purified from excess salt and potential oligomeric species using gel filtration on a size exclusion column (Superdex 75 10/300 GL, GE Healthcare) at a flow rate of 0.5 mL/min, and eluted in 20 mM sodium phosphate 0.2 mM EDTA buffer (at pH 8.0). The center of the peak was collected and the peptide concentration was determined from the averaged concentration using the Lambert-Beer equation

$$[A\beta_{42}] = \frac{OD_{start}+OD_{peak}}{2 \cdot l \cdot \varepsilon_{280}}$$

where OD is the optical density at 280 nm measured at the start and at the peak of the collection, ε_{280} is the is the molar absorptivity coefficient at 280 nm (for $A\beta_{42}$ ε_{280} = 1490 $M \cdot cm^{-1}$), and l=2 mm is the optical path length. The obtained peptide was diluted to the desired concentration with 20 mM sodium phosphate 0.2 mM EDTA buffer (pH 8.0) and supplemented with 20 μM ThT and different molar-equivalents of SUVs. All samples were prepared in low binding test tubes (Eppendorf, Hamburg, Germany) on ice. Each sample was then pipetted into multiple wells of a 96-well half-area, low-binding, clear bottom and PEG coating plate (Corning 3881, Corning, New York, NY, USA). Assays were initiated by placing the 96-well plate at 37 ºC under quiescent conditions in a plate reader (Fluostar Omega or Fluostar Optima, BMG Labtech). The ThT fluorescence was measured through the bottom of the plate with a 440 nm excitation filter and a 480 nm emission filter.

$A\beta_{42}$ fibrils quantification through dot blot. In order to either evaluate the kinetics of $A\beta_{42}$ aggregation in a ThT-free environment, dot blotting was performed as previously described[23], with a few variations. Briefly, during the time course aggregation of 2 μM $A\beta_{42}$ in 20 mM sodium phosphate 0.2 mM EDTA buffer (pH 8.0) non supplemented with ThT, 3 μL of reaction were spotted on a 0.2 μm pore size nitrocellulose membrane (Whatman, Maidstone, UK). The membrane was air-dried and blocked overnight (room temperature) with 5% skim milk in Phosphate Buffer Saline supplemented with 0.5% Tween20. The membrane was then stained with the $A\beta_{42}$ fibril specific OC antibody (Millipore, Billerica, MA, USA) and an Alexa Fluor 488-conjugated secondary antibody (Life Technologies, Carlsbad, CA, USA) was subsequently added. Fluorescence detection using an excitation wavelength of 488 nm was performed using a Typhoon Trio Imager (GE Healthcare).

Differential scanning calorimetry (DSC). In order to determine the T_m of selected lipid mixtures, DSC thermograms were acquired using a Microcal VP-DSC calorimeter (Malvern Instruments, Malvern, UK) with a scanning rate of 1 ºC from 13 ºC to 50 ºC. 1 mM SUV samples were degassed at room temperature for 20 minutes before acquisition of the DSC thermograms. All DSC thermograms were baseline-corrected by subtracting the phosphate buffer thermogram, normalized against the maximum value, and smoothened using a 2nd order 4-neighbors smoothing function from GraphPad Prism 8 (GraphPad Software, San Diego, CA, USA).

SUV-ssDNA gel electrophoresis. SUVs were incubated for 2 h with 10 nM of a 21-bases oligonucleotide in the native buffer. The ssDNA sequence (TAA GAC AGA TAC TAG CCT ACC) was ordered from Integrated DNA Technologies (Coralville, IA, USA) with a Cholesterol-TEG linker modification at the 3' end. The gel was prepared by adding 1.0 g Agarose (Sigma Aldrich, St. Louis, MO, USA) to a 11 mM MgCl2 solution buffered with 0.5x TBE (pH = 8). Samples were run for 100 min at 60 V alongside a 1kB DNA ladder (New England Biolabs, Ipswich, MA, USA). Imaging was performed by staining the gel in a GelRed (Biotium, Fremont, CA, USA) bath for 10 minutes followed by UV radiation.

Transmission electron microscopy imaging. For TEM imaging, a solution of 10 μM $A\beta_{42}$ in 20 mM sodium phosphate 0.2 mM EDTA buffer (pH 8.0) is incubated at 37ºC in a low-binding centrifuge tube (Eppendorf, Hamburg, Germany) in absence or presence of 500 μM 4LM (POPE, POPC, POPS, POPG) or 500 μM 4LM supplemented with 10% cholesterol SUVs. Reaching of plateau was monitored in a plate reader using analogous samples of 10 μM $A\beta_{42}$ supplemented with 20 μM ThT pipetted in a Corning 3881 96-wells plate. After the endpoint of the reaction was reached, fibrils were centrifuged on a benchtop centrifuge (15 min, 15000 g, 4 ºC) and resuspended in the same phosphate buffer to obtain a solution of ~200 μM. A 5 μL sample of the concentrated fibrils is applied to carbon-coated 400-mesh copper grids (EM Resolutions, Saffron Walden, UK). Samples were washed with deionised water in order to avoid the presence of liposome-induced artefacts and then stained with 2% (w/v) uranyl acetate and imaged using a FEI Talos F200X G2 transmission electron microscope (Electron Microscopy Facility in the Department of Chemistry, University of Cambridge, UK).

ASSOCIATED CONTENT

Supporting Information

The Supporting Information is available free of charge on the ACS Publications website.

Additional figures (PDF)

AUTHOR INFORMATION

Corresponding Author
***E-mail: mv245@cam.ac.uk.**
ORCID
Michele Vendruscolo: 0000-0002-3616-1610
Michele Sanguanini: 0000-0002-7142-3807

Funding Sources

This work was supported by the Centre for Misfolding Diseases.

Authors Contributions

M.S. and M.V. designed research; M.S., K.N.B., S.P., S.C., J.H. performed research. M.S., K.N.B., S.P., S.C., J.H., T.P.J.K and M.V analysed the data. M.S., K.N.B., S.P., S.C., J.H., T.P.J.K and M.V wrote the paper.

REFERENCES

(1) Hayden, K. M.; Inouye, S. K.; Cunningham, C.; Jones, R. N.; Avidan, M. S.; Davis, D.; Kuchel, G. A.; Tang, Y.; Khachaturian, A. S. Reduce the Burden of Dementia Now. *Alzheimer's Dement.* **2018**, *14* (7), 845–847. https://doi.org/10.1016/j.jalz.2018.06.3039.

(2) Selkoe, D. J.; Hardy, J. The Amyloid Hypothesis of Alzheimer's Disease at 25 Years. *EMBO Mol. Med.* **2016**, *8* (6), 595–608. https://doi.org/10.15252/emmm.201606210.

(3) Cleary, J. P.; Walsh, D. M.; Hofmeister, J. J.; Shankar, G. M.; Kuskowski, M. A.; Selkoe, D. J.; Ashe, K. H. Natural Oligomers of the Amyloid-β Protein Specifically Disrupt Cognitive Function. *Nat. Neurosci.* **2005**, *8* (1), 79–84. https://doi.org/10.1038/nn1372.

(4) Lesné, S.; Ming, T. K.; Kotilinek, L.; Kayed, R.; Glabe, C. G.; Yang, A.; Gallagher, M.; Ashe, K. H. A Specific Amyloid-β Protein Assembly in the Brain Impairs Memory. *Nature* **2006**, *440* (7082), 352–357. https://doi.org/10.1038/nature04533.

(5) Koffie, R. M.; Meyer-Luehmann, M.; Hashimoto, T.; Adams, K. W.; Mielke, M. L.; Garcia-Alloza, M.; Micheva, K. D.; Smith, S. J.; Kim, M. L.; Lee, V. M.; Bradley T. H.; Spires-Jones, T. L. Oligomeric Amyloid β Associates with Postsynaptic Densities and Correlates with Excitatory Synapse Loss near Senile Plaques. *Proc. Natl. Acad. Sci.* **2009**, *106* (10), 4012–4017. https://doi.org/10.1073/pnas.0811698106.

(6) Hipp, M. S.; Park, S. H.; Hartl, U. U. Proteostasis Impairment in Protein-Misfolding and Aggregation Diseases. *Trends Cell Biol.* **2014**, *24* (9), 506–514. https://doi.org/10.1016/j.tcb.2014.05.003.

(7) Knowles, T. P. J.; Vendruscolo, M.; Dobson, C. M. The Amyloid State and Its Association with Protein Misfolding Diseases. *Nat. Rev. Mol. Cell Biol.* **2014**, *15* (6), 384–396. https://doi.org/10.1038/nrm3810.

(8) Lindquist, S. L.,; Kelly, J. W. Chemical and Biological Approaches for Adapting Proteostasis to Ameliorate Protein Misfolding and Aggregation Diseases: Progress and Prognosis. *Cold Spring Harb. Perspect. Biol.* **2011**, *3* (12), a004507.

(9) Hipkiss, A. R.; Cartwright, S. P.; Bromley, C.; Gross, S. R.; Bill, R. M. Carnosine: Can Understanding Its Actions on Energy Metabolism and Protein Homeostasis Inform Its Therapeutic Potential? *Chem. Cent. J.* **2013**, *7* (1), 1–9. https://doi.org/10.1186/1752-153X-7-38.

(10) Choi, J.; Yin, T.; Shinozaki, K.; Lampe, J. W. Comprehensive Analysis of Phospholipids in the Brain, Heart, Kidney, and Liver : Brain Phospholipids Are Least Enriched with Polyunsaturated Fatty Acids. *Mol. Cell. Biochem.* **2018**, *442* (1), 187–201. https://doi.org/10.1007/s11010-017-3203-x.

(11) Aisenbrey, C.; Borowik, T.; Byström, R.; Bokvist, M.; Lindström, F.; Misiak, H.; Sani, M. A.; Gröbner, G. How Is Protein Aggregation in Amyloidogenic Diseases Modulated by Biological Membranes? *Eur. Biophys. J.* **2008**, *37* (3), 247–255. https://doi.org/10.1007/s00249-007-0237-0.

(12) Matsuzaki, K. How Do Membranes Initiate Alzheimers Disease? Formation of Toxic Amyloid Fibrils by the Amyloid beta-Protein on Ganglioside Clusters. *Acc. Chem. Res.* **2014**, *47* (8), 2397–2404. https://doi.org/10.1021/ar500127z.

(13) Habchi, J.; Chia, S.; Galvagnion, C.; Michaels, T. C. T.; Bellaiche, M. M. J.; Ruggeri, F. S.; Sanguanini, M.; Idini, I.; Kumita, J. R.; Sparr, E.; Linse, S.; Dobson, C. M.; Knowles, T. P. J.; Vendruscolo, M. Cholesterol Catalyses Aβ42 Aggregation through a Heterogeneous Nucleation Pathway in the Presence of Lipid Membranes. *Nat. Chem.* **2018**, *10* (6), 673–683. https://doi.org/10.1038/s41557-018-0031-x.

(14) Galvagnion, C.; Brown, J. W. P.; Ouberai, M. M.; Flagmeier, P.; Vendruscolo, M.; Buell, A. K.; Sparr, E.; Dobson, C. M. Chemical Properties of Lipids Strongly Affect the Kinetics of the Membrane-Induced Aggregation of α-Synuclein. *Proc. Natl. Acad. Sci.* **2016**, *113* (26), 7065–7070. https://doi.org/10.1073/pnas.1601899113.

(15) Korshavn, K. J.; Satriano, C.; Lin, Y.; Zhang, R.; Dulchavsky, M.; Bhunia, A.; Ivanova, M. I.; Lee, Y. H.; La Rosa, C.; Lim, M. H.; Ramamoorthy, A. Reduced Lipid Bilayer Thickness Regulates the Aggregation and Cytotoxicity of Amyloid-β. *J. Biol. Chem.* **2017**, *292* (11), 4638–4650. https://doi.org/10.1074/jbc.M116.764092.

(16) Cheng, Q.; Hu, Z. W.; Doherty, K. E.; Tobin-Miyaji, Y. J.; Qiang, W. The On-Fibrillation-Pathway Membrane Content Leakage and off-Fibrillation-Pathway Lipid Mixing Induced by 40-Residue β-Amyloid Peptides in Biologically Relevant Model Liposomes. *Biochim. Biophys. Acta - Biomembr.* **2018**, *1860* (9), 1670–1680. https://doi.org/10.1016/j.bbamem.2018.03.008.

(17) Österlund, N.; Kulkarni, Y. S.; Misiaszek, A. D.; Wallin, C.; Krüger, D. M.; Liao, Q.; Mashayekhy Rad, F.; Jarvet, J.; Strodel, B.; Wärmländer, S. K. T. S.; Ilag, L. L.; Kamerlin, S. C. L.; Graslund A. Amyloid-β Peptide Interactions with Amphiphilic Surfactants: Electrostatic and Hydrophobic Effects. *ACS Chem. Neurosci.* **2018**, *9* (7), 1680–1692.

https://doi.org/10.1021/acschemneuro.8b00065.

(18) Gaspar, R.; Pallbo, J.; Weininger, U.; Linse, S.; Sparr, E. Ganglioside Lipids Accelerate α-Synuclein Amyloid Formation. *Biochim. Biophys. Acta - Proteins Proteomics* **2018**, *1866* (10), 1062–1072. https://doi.org/10.1016/j.bbapap.2018.07.004.

(19) Ryan, T. M.; Griffin, M. D. W.; Teoh, C. L.; Ooi, J.; Howlett, G. J. High-Affinity Amphipathic Modulators of Amyloid Fibril Nucleation and Elongation. *J. Mol. Biol.* **2011**, *406* (3), 416–429. https://doi.org/10.1016/j.jmb.2010.12.023.

(20) Feller, W. *An Introduction to Probability Theory and Its Applications*; John Wiley & Sons, New York-London-Sydney, 2008.

(21) Cohen, S. I. A.; Linse, S.; Luheshi, L. M.; Hellstrand, E.; White, D. a; Rajah, L.; Otzen, D. E.; Vendruscolo, M.; Dobson, C. M.; Knowles, T. P. J. Proliferation of Amyloid-B42 Aggregates Occurs through a Secondary Nucleation Mechanism. *Proc. Natl. Acad. Sci. U. S. A.* **2013**, *110* (24), 9758–9763. https://doi.org/10.1073/pnas.1218402110.

(22) Arosio, P.; Vendruscolo, M.; Dobson, C. M.; Knowles, T. P. J. Chemical Kinetics for Drug Discovery to Combat Protein Aggregation Diseases. *Trends Pharmacol. Sci.* **2014**, *35* (3), 127–135. https://doi.org/10.1016/j.tips.2013.12.005.

(23) Habchi, J.; Arosio, P.; Perni, M.; Costa, A. R.; Yagi-Utsumi, M.; Joshi, P.; Chia, S. K. R.; Cohen, S. I. A.; Müller, M. B. .; Linse, S.; Nollen, E. A. A.; Dobson, C. M.; Tuomas P. J. Knowles, T. P. J.; Vendruscolo, M. An Anti-Cancer Drug Suppresses the Primary Nucleation Reaction That Initiates the Formation of Toxic Aβ Aggregates Associated with Alzheimer's Disease. *Sci. Adv.* **2015**, 2 (2), e1501244. https://doi.org/10.1126/sciadv.1501244.

(24) Cohen, S. I. A.; Arosio, P.; Presto, J.; Kurudenkandy, F. R.; Biverstål, H.; Dolfe, L.; Dunning, C.; Yang, X.; Frohm, B.; Vendruscolo, M.; Johansson, J.; Dobson, C. M.; Fisahn, A.; Knowles, T. P. J.; Linse, S. A Molecular Chaperone Breaks the Catalytic Cycle That Generates Toxic Aβ Oligomers. *Nat. Struct. Mol. Biol.* **2015**, *22* (3), 207–213. https://doi.org/10.1038/nsmb.2971.

(25) Arosio, P.; Michaels, T. C. T.; Linse, S.; Månsson, C.; Emanuelsson, C.; Presto, J.; Johansson, J.; Vendruscolo, M.; Knowles, T. P. J.; Dobson, C. M. Kinetic Analysis Reveals the Diversity of Microscopic Mechanisms through Which Molecular Chaperones Suppress Amyloid Formation. *Nat. Commun.* **2016**, *7* (1), 1–9. https://doi.org/10.1038/ncomms10948.

(26) Aprile, F. A.; Sormanni, P.; Perni, M.; Arosio, P.; Linse, S.; Knowles, T. P. J.; Dobson, C. M.; Vendruscolo, M. Selective Targeting of Primary and Secondary Nucleation Pathways in Ab42 Aggregation Using a Rational Antibody Scanning Method. *Sci. Adv.* **2017**, *3* (6), e1700488. https://doi.org/10.1126/sciadv.1700488.

(27) Chia, S.; Flagmeier, P.; Habchi, J.; Lattanzi, V.; Linse, S.; Dobson, C. M.; Knowles, T. P. J.; Vendruscolo, M. Monomeric and Fibrillar α-Synuclein Exert Opposite Effects on the Catalytic Cycle That Promotes the Proliferation of Aβ42 Aggregates. *Proc. Natl. Acad. Sci.* **2017**, *114* (30), 8005–8010. https://doi.org/10.1073/pnas.1700239114.

(28) De Cuyper, M.; Joniau, M.; Engberts, J. B. F. N.; Sudholter, E. J. R. Exchangeability of Phospholipids between Anionic, Zwitterionic and Cationic Membranes. *Colloids and Surfaces* **1984**, *10* (C), 313–319. https://doi.org/10.1016/0166-6622(84)80032-3.

(29) Janosi, L.; Gorfe, A. A. Simulating POPC and POPC/POPG Bilayers: Conserved Packing and Altered Surface Reactivity. *J. Chem. Theory Comput.* **2010**, *6* (10), 3267–3273. https://doi.org/10.1021/ct100381g.

(30) Ege, C.; Majewski, J.; Wu, G.; Kjaer, K.; Lee, K. Y. C. Templating Effect of Lipid Membranes on Alzheimer's Amyloid Beta Peptide. *ChemPhysChem* **2005**, *6* (2), 226–229. https://doi.org/10.1002/cphc.200400468.

(31) Sastry, P. S. Lipids of Nervous Tissue: Composition and Metabolism. *Progress in Lipid Research*. 1985, pp 69–176. https://doi.org/10.1016/0163-7827(85)90011-6.

(32) Chan, R. B.; Oliveira, T. G.; Cortes, E. P.; Honig, L. S.; Duff, K. E.; Small, S. A.; Wenk, M. R.; Shui, G.; Di Paolo, G. Comparative Lipidomic Analysis of Mouse and Human Brain with Alzheimer Disease. *J. Biol. Chem.* **2012**, *287* (4), 2678–2688. https://doi.org/10.1074/jbc.M111.274142.

(33) Lewis, K. T.; Maddipati, K. R.; Naik, A. R.; Jena, B. P. Unique Lipid Chemistry of Synaptic Vesicle and Synaptosome Membrane Revealed Using Mass Spectrometry. *ACS Chem. Neurosci.* **2017**, *8* (6), 1163–1169. https://doi.org/10.1021/acschemneuro.7b00030.

(34) Sasahara, K.; Morigaki, K.; Shinya, K. Effects of Membrane Interaction and Aggregation of Amyloid β-Peptide on Lipid Mobility and Membrane Domain Structure. *Phys. Chem. Chem. Phys.* **2013**, *15* (23), 8929–8939. https://doi.org/10.1039/c3cp44517h.

(35) Walsh, D. M.; Thulin, E.; Minogue, A. M.; Gustavsson, N.; Pang, E.; Teplow, D. B.; Linse, S. A Facile Method for Expression and Purification of the Alzheimer's Disease-Associated Amyloid β-Peptide. *FEBS J.* **2009**, *276* (5), 1266–1281. https://doi.org/10.1111/j.1742-4658.2008.06862.x.

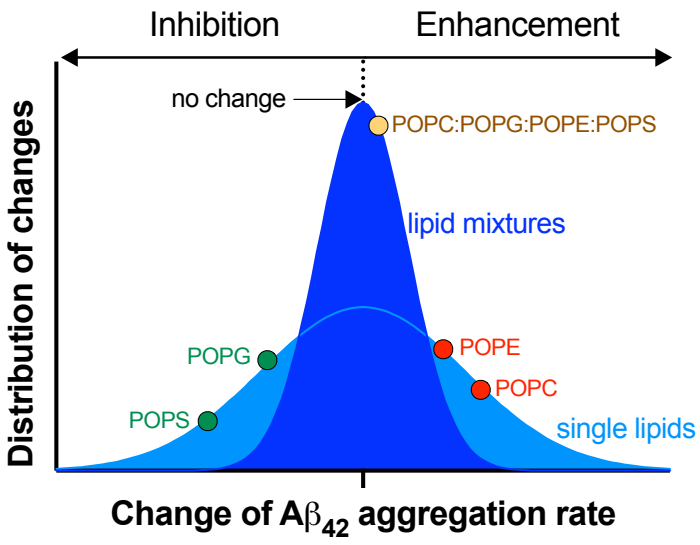

Table of Contents Graphic